ISSN 8755-6839

SCIENCE OF **TSUNAMI HAZARDS**

Journal of Tsunami Society International

Volume 40 **Number 3** **2021**

TSUNAMI FAULTING MODEL ANALYSIS FOR THE 30 OCTOBER 2020 NORMAL EARTHQUAKE OCCURRED IN IZMIR-TURKEY

Madlazim[1,*], Eko Hariyono[1], Muhammad Nurul Fahmi[1], Dyah Permata Sari[1]

[1] Department of Physics, Faculty of Mathematics and Natural Sciences, Universitas Negeri Surabaya, Surabaya 60231, Indonesia
*Correspondence: madlazim@unesa.ac.id

ABSTRACT

This study aims to analyse the M_w 7.0 normal faulting type earthquake that occurred on October 30, 2020, in Izmir-Turkey. After the earthquake, a tsunami was followed with a maximum water level of 3.8 meters in the Aegean Sea. The used method in this study is the measurement of the tsunami faulting model parameters by using a direct procedure. The measured tsunami parameters are the dominance period (T_d), rupture duration (T_{dur}), and rupture duration more than 50 seconds (T_{50Ex}) as well as the results of the multiplication between T_d and T_{50Ex} (T_dT_{50Ex}). In this study, we used seismogram velocity of vertical component recorded by the Global Seismographic Networks (GSN) network stations and the GEOFON (GE) network with an epicenter distance of 0 to 40°, totaling 66 seismic stations. Based on the measurement results, the tsunami discriminants T_{dur} = 65.11 seconds, T_d = 9.28 seconds, T_{50Ex} = 1.43 and T_dT_{50Ex} = 13.27 seconds > 10 seconds (threshold). The value of the tsunami discriminants T_dT_{50Ex} that exceeds this threshold strengthens that the normal type earthquake is the cause of the tsunami.

Key words: *Normal earthquake, dominant period, rupture duration, rupture duration more than 50 seconds, tsunami faulting model.*

Vol. 40, No. 3, page 196 (2021)

1. INTRODUCTION

Worldwide tsunamis caused by earthquakes are more often caused by reverse fault earthquakes than those caused by normal earthquakes and strike-slip earthquakes. This is understandable because the vertical displacement component of a reverse earthquake is much larger than that of a normal and strike-slip earthquake. Large tsunamis are rarely generated by strike-slip or normal-faulting events. This is because strike-slip faults that trigger local tsunamis may only be correlated with the size of the localized seafloor deformation insignificantly (Gusman, et al., 2017; Lay et al., 2017). However, records of past tsunamis initiated by strike-slips are reported as, for example, in 1906 in San Francisco, California (Ma, et al., 1991; Thatcher, et al., 1997) and in 1994 in Mindoro, Philippines (Imamura et al., 1995). These examples are complemented by relatively recent events in 2016 in Kaikoura, New Zealand (Power et al., 2017; Ulrich, et al., 2019a), and in Palu on 28 of September 2018, Indonesia (Carvajal, et al., 2019; Ulrich et al., 2019b; Madlazim, et al., 2020). From the total 35 events used in the study, Madlazim et al. (2021), found that 74% (26 events of normal and strike-slip earth quakes), have been validated to cause tsunamis, of which 11 strike-slips and 15 normal earthquakes. Therefore, these two mechanisms can be a potential source of tsunami generation.

On the coast near the Aegean Sea, densely populated coastal areas have been affected by several tsunamis in the past, some of them were devastating (Altinok et al., 2011; Altinok & Ersoy, 2000; Ambraseys & Synolakis, 2010; Papadopoulos et al., 2014; Dogan et al., 2021). The most famous tsunami in this region was the 1956 Amorgos event (M_w 7.8) which caused a maximum run up water level of up to 25 m (Beisel et al., 2009; Okal, el al., 2009). More recently, the eastern Aegean Sea was the site of two tsunamis that followed by the occurrence of earthquakes measuring M_w 6.3 and 6.6 respectively in June and July 2017. Both at Lesvos on 12 of June 2017 and at Bodrum-Kos on July 212020,, 2017, which was followed by a tsunami from a medium-magnitude earthquake in the region. The latter event caused a significant impact on the southern coast of the Bodrum Peninsula in Turkey and the Port of Kos on Kos Island in Greece (Dogan et al., 2019, 2021).

A strong earthquake that occurred on October 30, 2020, with a magnitude of M_w 6.6 has hit Samos Island in Greece and Izmir Province in Turkey in the eastern Aegean. Based on information from the Kandilli Observatory and Earthquake Research Institute (KOERI) and Anadolu Agency that this Tsunami occurred after the earthquake and caused significant damage in Cesme and Seferihisar Districts in Izmir and the coast of the Samos Island, and resulted in one victim and several injured people due to the tsunami on the Turkish side. The national tsunami warning centre and tsunami service for the North-East Atlantic, the Mediterranean Ocean Tsunami Warning System and the Ocean Connected System (NEAMTWS), issues a tsunami warning 11 minutes after the earthquake (Dogan et al., 2021). In this paper, we present the results of the velocity seismogram of vertical component data analysis from the 30 of October 2020 earthquake that occurred in Izmir-Turkey to confirm that the tsunami was caused by the earthquake. Our results include: measurement of dominance period (T_d), rupture duration (T_{dur}), and rupture duration more than 50 seconds (T_{50Ex}) as well as the results of the multiplication of T_d and T_{50Ex} (T_dT_{50Ex}). Next, we discuss the findings in this study to deeply understand the behavior of the tsunami and its impact on nearby coastal areas.

2. TECTONIC SETTING

The cause of the Turkish earthquake on October 30 include the many shifts in tectonic plates and other seismic forces that play a major role in the region for frequent earthquakes (National Geographic, 31/10/2020). An earthquake with an earlier estimated magnitude of 7 struck near the city of Izmir in 1688. It changed the landscape so much that the surface dropped by more than a foot, and the shaking buildings collapsed and started fires and killed up to 16,000 people. The eastern Aegean Sea region is characterized as dominated by dip-slip extensional tectonic (Aktar, et al., 2007). The Aegean Sea coasts of Turkey and Greece were struck by a moderate tsunami on 30 October 2020, which was generated by an M_w 7.0 normal-faulting earthquake (Fig. 1).

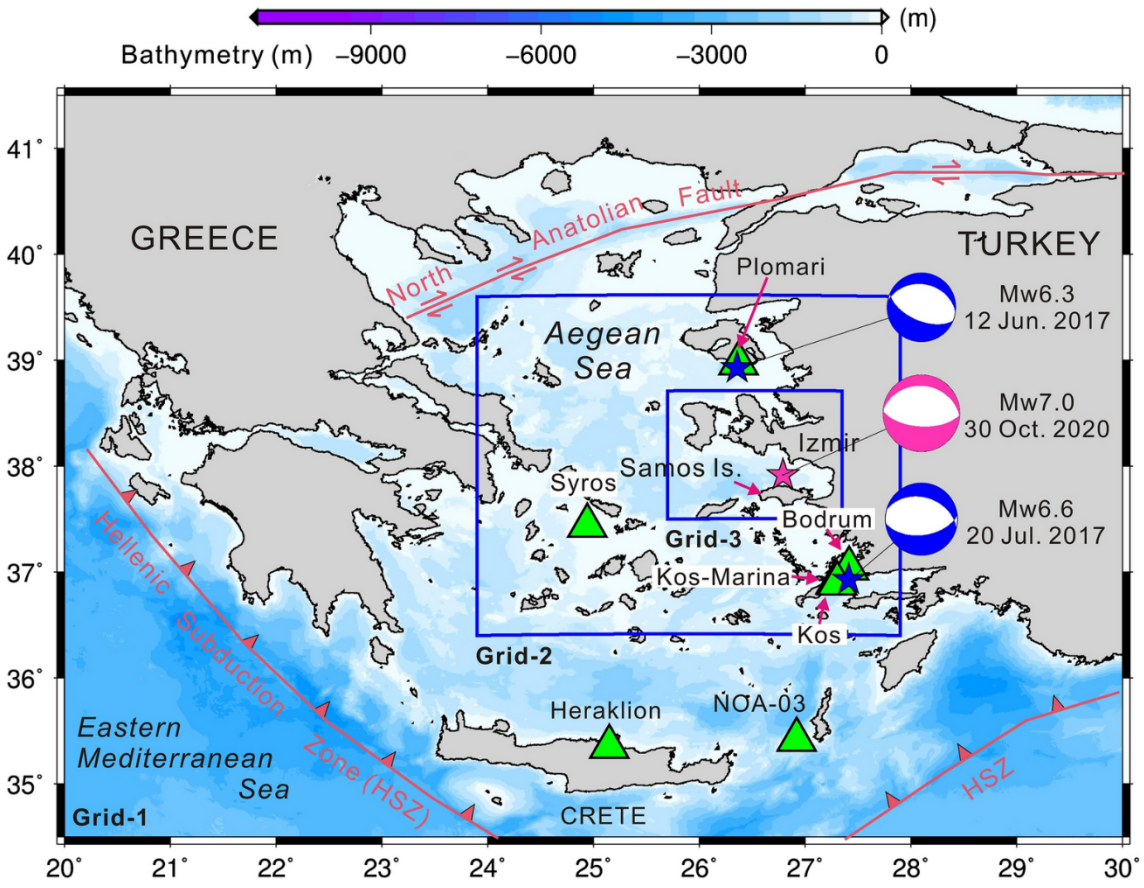

Figure 1. Tectonic setting of the Aegean Sea region and the epicentral area of the 30 October 2020 Mw 7.0 earthquake. Data of epicenters and focal mechanisms belong to the United States Geological Survey (USGS) earthquake catalogue. Green triangles show the locations of tide gauges. The blue boxes show the geographical areas of Grid-2 (spatial resolution = 10.8 arc-sec) and Grid-3 (spatial resolution = 3.6 arc-sec), which form the nested grid system that we used for numerical modelling of the tsunami (Heidarzadeh et al., 2021).

These include faults trending E–W according to their area extending in the N–S direction and showing a dextral (right-lateral) or sinistral (left-lateral) component (Emre, et al., 2011; Tan et al., 2014; Tepe & Sözbilir, 2017). Therefore, the tsunami threat in the study area is mainly associated with the dominant normal fault which indicates a high potential risk for the coastal area. On October 30, 2020, 12:51 UTC (14:51 local time), an underwater earthquake (M_w 6.6) occurred in north of Samos Island, Greece, and off the coast of Seferihisar-Izmir, Turkey, with an epicenter (37.88 N , 26.70 E) at a depth of 15 km (AFAD, 2020). More than 4600 aftershocks have occurred by the end of November 2020, 50 of them had a magnitude of M_w 4.0. The largest was with a magnitude of M_w 5.1 occurred at 16:14 (UTC), about 4 hours after the earthquake, about 10 km southeast of the epicenter at a depth of about 7 km. From the conjugate-type aftershock distribution between the Dilek Peninsula (DP) in Turkey and the northern Greek Island of Ikaria, about 80–100 km long rupture crack in the E–W direction is clearly visible in four segments with visible seismic gaps. Three segments are located in the northern part of Samos, while the eastern part of the swarm is aligned in the NNE–SSW direction, which is parallel to the Buyuk Menderes Graben (BMG) alignment. north of Kusadasi Bay (KB) and western part of Samos reveal a diffuse type of seismic activity (Dogan et al., 2021).

3. METHOD

There are two models of earthquake faults that have been used to explain the source of earthquakes.

Examination of the first examine earthquake faulting model: This theory explains the relationship between the strength (magnitude, M_w or seismic moment, M_0) of the earthquake source and the fault length, L, fault width, W, slip, D and shear modulus, as written in the equation M_0 = LWD. This model inspired seismologists that M_0 or M_w could be used as an early warning for earthquakes and tsunamis. The use of M_w or M_0 based on this model for earthquake early warning is quite accurate, but for tsunami early warning it still needs to be evaluated. The second model is the tsunami faulting model. After finding that the earthquake faulting model was not accurate for tsunami early warning, Lomax & Michelini (2011) developed a tsunami faulting model inspired by Satake's (1994) theory. This model provides the basis that not all earthquakes with a moment magnitude, M_w > 7 cause tsunamis because tsunami events still depend on the parameters of rupture length (L) and rupture width (W). This model also illustrates that the longer the earthquake rupture (L), the shallower the depth (z) of the earthquake centre. This can be explained based on the relationship between depth, density of the earth's medium and the shear modulus. The shallower the earth medium, the sparser the density and the smaller the value of the shear modulus, so that the rupture length is greater for certain earthquakes. The rupture length (L) is proportional to the rupture duration (T_{dur}). The rupture length is difficult to be measured directly, while T_{dur}, T_d and T_{50Ex} can be measured directly from a seismogram,

so tsunami early warning is very possible by using the tsunami parameters T_{dur}, T_d and T_{50Ex}. Threshold T_d 10 s, T_{dur}=65 s, T_{50Ex}, T_d*T_{dur}= 650 s^2 and T_d*T_{50Ex}= 10 s (Madlazim, 2013; Madlazim, et al. 2015). If the measurement results of the tsunami parameters exceed the threshold, then the earthquake has the potential to cause a tsunami.

3.1. *Rupture Duration of* P Wave (T_{dur})

High-frequency seismograms contain a larger number of P wave phase groups, so that the search for earthquake rupture duration represented by P wave groups fulfills the representative requirements in estimating the wave rupture duration for P tele-seismic earthquakes (Lomax & Michelini, 2009c). The algorithms used to estimate the rupture duration of a regional earthquake seismogram are: (1) providing a seismogram of the vertical component of the ground motion velocity in miniseed format as raw data; (2) applying a 4-pole and a 5–20 Hz Butterworth band-pass filter to obtain a vertical seismogram recording speed on HF for each Indonesian local station network; (3) converting the HF seismogram into velocity-squared envelopes to get the rms amplitude; (4) picking the arrival time of the P wave automatically on the HF seismogram; (5) measuring the time delay after the arrival of the P wave for 90%($T^{0,9}$), 80%($T^{0,8}$), 50%($T^{0,5}$) and 20% ($T^{0,2}$) of the peak value; and (6) calculating the rupture duration, T_{dur} for that station by using the equation:

$$T_{dur} = (1 - w)T^{0.9} + wT^{0.2} \quad (1)$$

with,

$$w = \left[\left(T^{0.8} + T^{0.5}\right)/2 - 20\right]/40\ s \quad (2)$$

and the value of w is constrained $0 \leq w \leq 1$ (Lomax & Michelini, 2009a) ; (7) plot $T^{0,2}$, $T^{0,5}$, $T^{0,8}$, $T^{0,9}$ and T_{dur} in the seismogram.

3.2. *Rupture Duration of* P Wave (T_{dur})

First of all, calculate the time domain (tc) by using the following equation :

$$\tau_c = 2\pi \int_{T_2}^{T_1} v^2(t)dt / \int_{T_2}^{T_1} \acute{v}^2(t)dt \quad (3)$$

(Nakamura, 1988; Wu & Kanamori, 2005: Lomax & Michelini, 2013)

With T_1 = 0 seconds (P onset) and T_2 = 55 seconds for tele seismic earthquake seismograms (Lomax and Michelini, 2009). Detailed steps of T_d estimation are as follows: (1) preparing raw earthquake data records from the vertical velocity component of broadband seismogram in a miniseed format, (2)

applying 4-poles and a corner frequency of 0.05 Hz Butterworth band pass filter to obtain the high-frequency, vertical component of velocity records for each seismic station; (3) picking *P*-wave arrival times automatically at the high-frequency, vertical-velocity seismogram; (4) integrating the seismogram and comparing it with vertical acceleration component of broadband seismogram times 2π of arrival times of *P*-waves automatically picked up from the vertical-velocity records on the high-frequency seismogram; and (5) the final results were values of T_d.

3.3. Exceed Duration More Than 50 Seconds (T_{50Ex})

T_{50Ex} estimation was carried out by using a direct procedure for tele seismic earthquakes, namely (1) filtering the seismogram velocity of vertical component by using a high frequency (1–5 Hz) Butterworth filter, (2) automatically picking P wave arrival times, (3) calculating rms amplitude (Ar) and T_{50}, (4) calculating T_{50Ex} which is the ratio between T_{50}/A_r (Lomax & Michelini, 2009a). Furthermore, the equations generated from the faulting tsunami model are integrated into the Jokotingkir software (Madlazim, 2017).

4. FAULTING MODEL APPLICATION FOR THE 30 OCTOBER 2020 EARTHQUAKE IN TURKEY

Measurement of three tsunami parameters from the faulting tsunami model (T_{dur}, T_d, and T_{50Ex}) for the M_w 7.0 normal faulting type earthquake that occurred in Turkey on October 30, 2020 by using seismogram velocity of vertical component data recorded by 61 to 64 seismic stations on the GSN network and GE with a regional epicentral distance of 4° to 40° as shown in Figure 2.

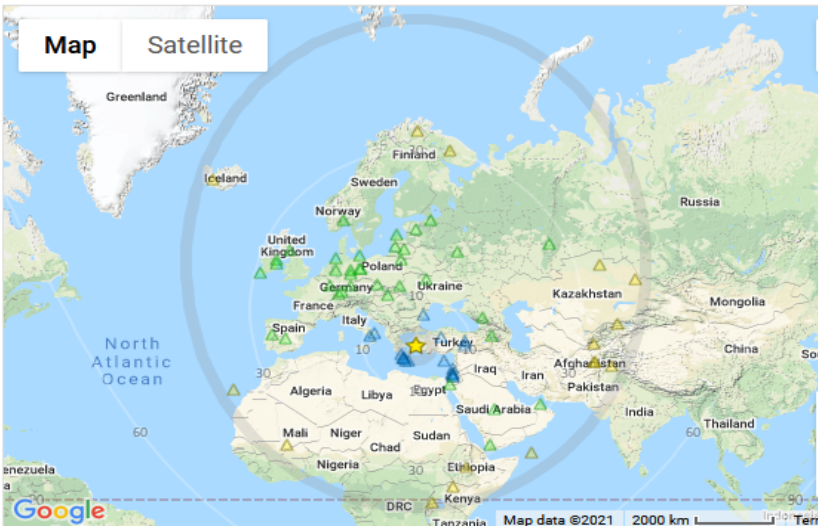

Figure 2. Distribution of seismic stations on the GSN network (green) and GE network (blue) and the epicenter of the M_w = 7 earthquake that occurred in Turkey on October 30, 2020.

5. RESULTS AND DISCUSSION

The results obtained in this study are the results of measuring three tsunami parameters from the tsunami faulting model (T_{dur}, T_d, and T_{50Ex}) for the M_w 7.0 normal faulting type earthquake that occurred in Turkey on October 30, 2020. From the results of the tsunami parameters calculation by using software Jokotingkir (Madlazim, 2017) whose real time application system can be accessed at http://predik-tsunami.unesa.ac.id/www/, the results are as shown in Table 1 below.

Table 1. Result of tsunami parameters calculation by using Joktingkir software

Tsunami Parameter	Number of Used Station	Value	Threshold	Decision
T_{dur}	61	65.11 s	50 s	-
T_d	64	9.28 s	10 s	-
T_{50Ex}	63	1.43	1	-
T_dT_{50Ex}	-	13.28 s	10 s	Tsunami

The number of stations used by each tsunami parameter is different because there are seismograms that do not meet the minimum requirements for each seismogram recorded by these seismic stations. Almost all tsunami parameter values exceed the threshold value, except for the dominant period (T_d) which is slightly smaller than the threshold. For the purposes of predicting a tsunami 4 minutes after the earthquake, T_{dur} is represented by T_{50Ex} because the computational T_{50Ex} turns out to be more accurate (Lomax & Michelini, 2013). However, the discriminant tsunami (T_dT_{50Ex}) exceeds the threshold, so it can be concluded that the M_w 7.0 earthquake is a normal faulting type. The one occurred in Turkey on October 30, 2020, was caused by the seismic energy of the earthquake, not a landslide or others (Dogan et al., 2021). This evidence confirms that normal fault earthquakes can cause tsunamis (Lomax & Michelini, 2013; Madlazim et al., 2021). The tsunami caused by this earthquake can also be validated from the Tsunami Event Validity (TEV) published at http://dx.doi.org/10.7289/V5PN93H7.

Large shallow earthquakes produce the most destructive tsunamis where the epicenter is on a fault line along the seabed. Tectonic subduction and tectonic plate boundaries are areas that have the most potential to cause tsunamis. These collisions of tectonic plates in these highly seismic regions cause large earthquakes when the plates are moving and passing one another, tilting, offsetting, or displacing large areas of the ocean floor from just a few kilometers to 1,000 or more. This sudden,

large vertical displacement of the seabed disturbs the sea level and generates a destructive tsunami as the water is displaced. The earthquake lifts or lowers the seabed. A tsunami can occur when an earthquake causes a sudden vertical deformation of the seabed, displacing the overlying water from its equilibrium position. When a reverse earthquake moves suddenly, a tsunami can be generated if it is associated with a destructive or convergent plate boundary. This is due to the vertical component of the movement and sudden displacement.

Movements on normal faults (normal earthquakes) can also cause seafloor displacement, but if the ground moves from side to side, not much will happen to the water. Because the size of such an event is usually too small to produce a large tsunami. Conversely, if the land moves up or down, it displaces a large body of water. As the water tries to equalize itself, this displaced water will try to adjust itself in the form of waves. Earthquakes associated with subduction zones are very effective in generating tsunamis. Although most tsunamis are caused by underwater earthquakes, it should be noted that not all underwater earthquakes cause tsunamis: typically, an earthquake must be greater than 7.0 on the Richter scale in order to produce a destructive tsunami. Only from this intensity upwards, it is enough energy released to rapidly displace enough water to create a tsunami and the earthquake must have the epicenter near the earth's surface. The abnormally slow deformation (represented by rupture duration, dominant period, and rupture duration more than 50 seconds) at the earthquake tsunami source may be a manifestation of the weak zone viscoelasticity below the deep trench boundary.

Heidarzadeh et al., 2021 described that the arrival times of the maximum tsunami wave were up to 14.9 h after the first tsunami arrivals at each station. The duration of tsunami oscillation was from 19.6 h to > 90 h at various tide gauges. Spectral analysis revealed several peak periods for the tsunami; we identified the tsunami source periods as 14.2–23.3 min. The weak zone implied by large normal earthquakes such as the October 30, 2020, Turkish earthquake and other normal earthquakes may be the result of heating friction at the interface between boundaries of lithosphere (Kanamori, 1972). The structure here can be modeled by the thin lithosphere which is thickly lined in the weak zone. This structure offers an explanation, via speculative one, for such a slow earthquake (rupture duration exceeding the threshold). The thin lithosphere above the weak zone can rupture, possibly under its own weight, causing a tsunami.

Figures 3, 4, and 5 are Schematic of a single-station, each of which describes the process of measuring the rupture duration (T_{dur}), dominant period (T_d), and rupture duration more than 50 s (T_{50Ex}) processing for the 2020.10.30, M_w = 7.0, Dodecanese Island, Greece earthquake recorded by station GE.PSZ. at 11.19° GCD.

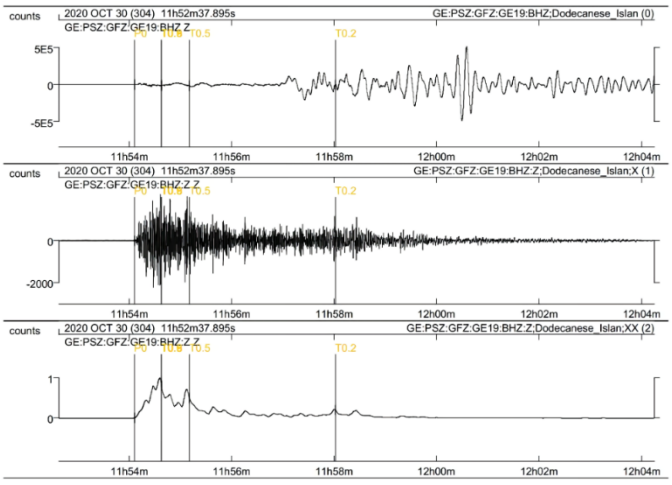

Figure 3. Schematic of a single-station, rupture duration (T_{dur}) processing for the 2020.10.30, M_w = 7.0, Dodecanese Island, Greece earthquake recorded by station GE.PSZ. at 11.19° GCD. Top panel represents raw, broadband velocity and the second panel is HF seismogram. The bottom panel is showing an estimation of T_{dur} = 82.69 s.

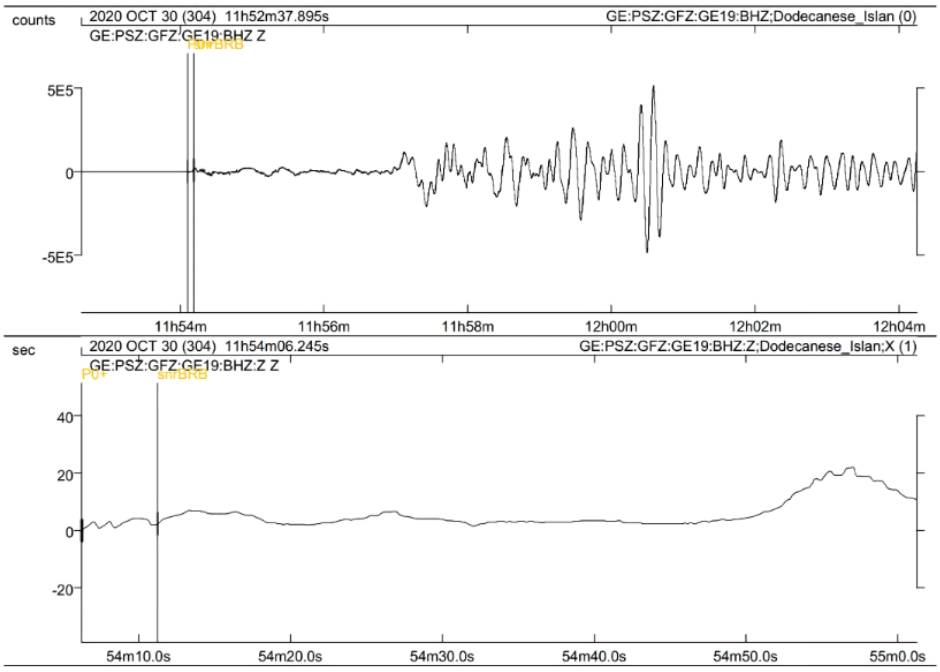

Figure 4. Schematic of a single-station, dominant period (T_d) processing for the 2020.10.30, M_w = 7.0, Dodecanese Island, Greece earthquake recorded by station GE.PSZ. at 11.19° GCD. Top panel represents raw broadband velocity. The bottom panel is showing an estimate of T_d = 22.35 s.

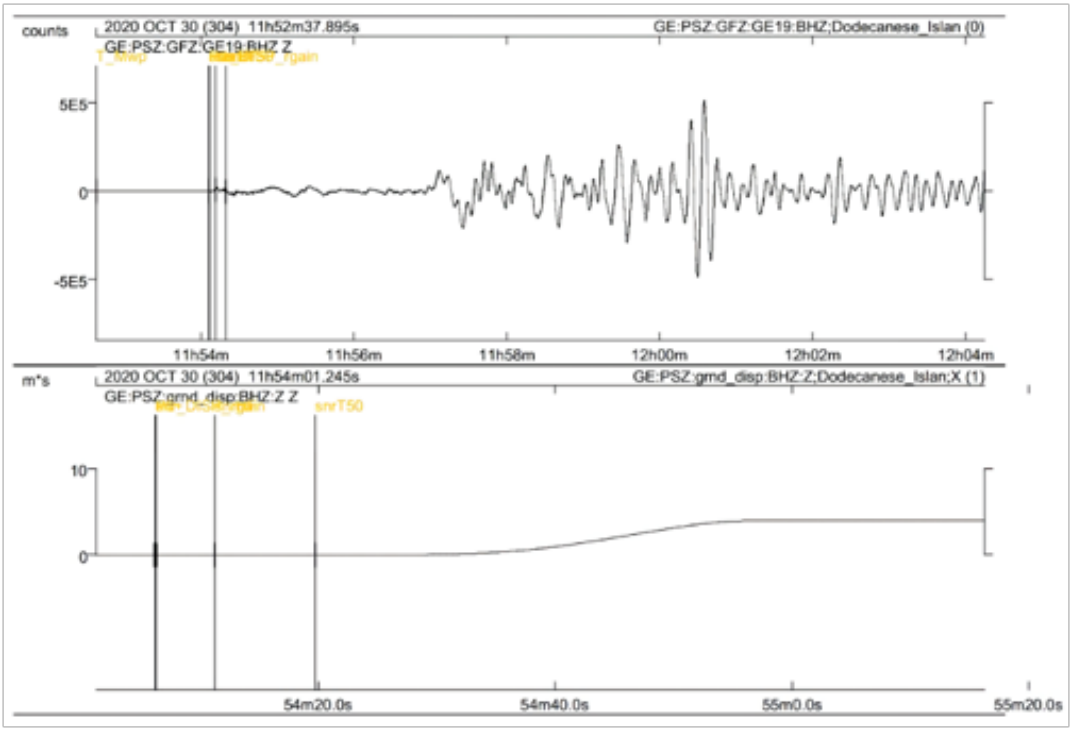

Figure 5. Schematic of a single-station, rupture duration more than 50 s (T_{50Ex}) processing for the 2020.10.30, M_w = 7.0, Dodecanese Island, Greece earthquake recorded by station GE.PSZ. at 11.19° GCD. Top panel represents raw broadband velocity. The bottom panel is showing an estimation of T_{50Ex} = 4.25 s.

6. CONCLUSIONS

Almost all tsunami parameter values exceed the threshold value, except for the dominant period (T_d) which is slightly smaller than the threshold. For the purpose of predicting a tsunami 4 minutes after the earthquake, T_{dur} is represented by T_{50Ex} because the computational T_{50Ex} turns out to be more accurate (Lomax, A. and Michelini, A., 2012). However, the discriminant tsunami (T_dT_{50Ex}) exceeds the threshold, so it can be concluded that the M_w 7.0 normal faulting type earthquake that occurred in Turkey on October 30, 2020, was caused by the seismic energy of the earthquake. Normal earthquakes can cause tsunamis because the thin lithosphere is thickly lined in the weak zone for very slow earthquakes (rupture duration, dominant period, and rupture duration exceeding the threshold). The thin lithosphere above the weak zone can rupture, possibly under its own weight, causing a tsunami.

ACKNOWLEDGEMENTS

The authors would sincerely like to thank the GEOFON GFZ and Incorporated Research Institutions for Seismology (IRIS) for which seismic data were freely available at http://eida.gfz-potsdam.de/webdc3/ and http://www.iris.edu/wilber3/find. This article is also beneficial from constructive reviews from two anonymous reviewers.

REFERENCES

AFAD (2020). Disaster and Emergency Management Authority (AFAD), Ministry of Interior, Ankara-Turkey. http://deprem. afad.gov.tr.

Aktar M, Karabulut H, Özalaybey S, Childs, D (2007). A conjugate strike-slip fault system within the extensional tectonics of Western Turkey. Geophysical Journal International 171(3): 1363–1375. https://doi.org/10.1111/j.1365-246X.2007.03598.x

Altinok Y, Alpar B, Özer N, Aykurt H (2011). Revision of the tsunami catalogue affecting Turkish coasts and surrounding regions. Natural Hazards and Earth System Science 11(2): 273–291. https://doi.org/10.5194/nhess-11-273-2011

Altinok Y, Ersoy Ş (2000). Tsunamis Observed on and Near the Turkish Coast. Natural Hazards 21(2): 185–205. https://doi.org/10.1023/A:1008155117243

Ambraseys N, Synolakis C (2010). Tsunami Catalogs for the Eastern Mediterranean, Revisited. Journal of Earthquake Engineering 14: 309–330. https://doi.org/10.1080/13632460903277593

Beisel S, Chubarov L, Didenkulova I, Kit E, Levin A, Pelinovsky E et al. (2009). The 1956 Greek tsunami recorded at Yafo, Israel, and its numerical modeling. Journal of Geophysical Research: Oceans 114(C9). https://doi.org/https://doi.org/10.1029/2008JC005262

Carvajal M, Araya-Cornejo C, Sepúlveda I, Melnick D, Haase JS (2019). Nearly Instantaneous Tsunamis Following the Mw 7.5 2018 Palu Earthquake. Geophysical Research Letters 46(10): 5117–5126. https://doi.org/https://doi.org/10.1029/2019GL082578

Dogan GG, Annunziato A, Papadopoulos GA, Guler HG, Yalciner AC, Cakir TE et al.2019). The 20 July 2017 Bodrum–Kos Tsunami Field Survey. Pure and Applied Geophysics 176(7): 2925–2949. https://doi.org/10.1007/s00024-019-02151-1

Dogan GG, Yalciner AC, Yuksel Y, Ulutaş E, Polat O, Güler I et al. (2021). The 30 October 2020 Aegean Sea Tsunami: Post-Event Field Survey Along Turkish Coast. Pure and Applied Geophysics 178(3): 785–812. https://doi.org/10.1007/s00024-021-02693-3

Emre Ö, Ozalp S, Duman TY (2011). 1:250,000 scale active fault map series of Turkey, I˙zmir (NJ 35-7) Quadrangle. In Serialnumber: 6. General Directorate of Mineral Research and Exploration, Ankara.

Gusman AR, Satake K, Harada T (2017). Rupture process of the 2016 Wharton Basin strike-slip faulting earthquake estimated from joint inversion of teleseismic and tsunami waveforms. Geophysical Research Letters 44(9): 4082–4089. https://doi.org/https://doi.org/10.1002/2017GL073611

Heidarzadeh, M., Pranantyo, I.R., Okuwaki, R. *et al.* Long Tsunami Oscillations Following the 30 October 2020 M_w 7.0 Aegean Sea Earthquake: Observations and Modelling. *Pure Appl. Geophys.* **178,** 1531–1548 (2021). https://doi.org/10.1007/s00024-021-02761-8

Imamura F, Synolakis CE, Gica E, Titov V, Listanco E, Lee, HJ (1995). Field survey of the 1994 Mindoro Island, Philippines tsunami. Pure and Applied Geophysics 144(3): 875–890. https://doi.org/10.1007/BF00874399

Kanamori H (1972). Mechanism of tsunami earthquakes. Physics of the Earth and Planetary Interiors 6(5): 346–359. https://doi.org/https://doi.org/10.1016/0031-9201(72)90058-1

Lay T, Ye L, Bai Y, Cheung KF, Kanamori H, Freymueller J et al. (2017). Rupture Along 400 km of the Bering Fracture Zone in the Komandorsky Islands Earthquake (MW 7.8) of 17 July 2017. Geophysical Research Letters 44(24): 12,112-161,169. https://doi.org/https://doi.org/10.1002/2017GL076148

Lomax A, Michelini A (2009a). Mwpd: A duration-amplitude procedure for rapid determination of earthquake magnitude and tsunamigenic potential from P waveforms. Geophysical Journal International 176(1): 200–214. https://doi.org/10.1111/j.1365-246X.2008.03974.x

Lomax A, Michelini A (2009b). Tsunami early warning using earthquake rupture duration. Geophysical Research Letters 36(9). https://doi.org/https://doi.org/10.1029/2009GL037223

Lomax A, Michelini A (2011). Tsunami early warning using earthquake rupture duration and P-wave dominant period: the importance of length and depth of faulting. Geophysical Journal International 185(1): 283–291. https://doi.org/10.1111/j.1365-246X.2010.04916.x

Lomax A, Michelini A (2013). Tsunami Early Warning Within Five Minutes. Pure and Applied Geophysics 170(9): 1385–1395. https://doi.org/10.1007/s00024-012-0512-6

Ma K-F, Satake K, Kanamori H (1991). The Origin Of The Tsunami Excited By The 1906 San Francisco Earthquake. Bulletin of the Seismological Society of America, 81(4): 1396–1397.

Madlazim (2017). Use of The Joko Tingkir Software for Rapid Determination of Tsunami Faulting Parameters Resulting From the Mw-7.8 Earthquake of March 2, 2016, in Southern Sumatra. Science of Tsunami Hazards 36(1): 41–48.

Madlazim (2013). Assessment of tsunami generation potential through rapid analysis of seismic parameters: Case study: Comparison of the Sumatra Earthquakes of 6 April and 25 October 2010. Science of Tsunami Hazards 32(1): 29-38.

Madlazim Prastowo T, Fahmi MN (2020). Estimation of rupture directivity, CMT and earthquake tsunami parameters and their correlation with the main source of the first tsunami wave, September 28, 2018. Science of Tsunami Hazards 39(4): 228–242.

Madlazim, Prastowo T, Fahmi MN, Sari DP, Melianda E, Koesoema S. (2021). Tsunamis from strike-slip and normal earthquakes and its relation with the product of dominant period and duration more than 50 seconds of earthquake P-wave. Science of Tsunami Hazards (Accepted).

Madlazim, Prastowo T, Hardy T (2015). VALIDATION OF JOKO TINGKIR SOFTWARE USING TSUNAMI IMPORTANCE. Science of Tsunami Hazards 34(3): 189–198.

Nakamura Y. (1988). On the urgent earthquake detection and alarm system (UrEDAS). In Proc. of the 9th World Conference on Earthquake Engineering; Tokyo-Kyoto, Japan.

Okal EA, Synolakis CE, Uslu B, Kalligeris N, Voukouvalas E (2009). The 1956 earthquake and tsunami in Amorgos, Greece. Geophysical Journal International 178(3): 1533–1554. https://doi.org/https://doi.org/10.1111/j.1365-246X.2009.04237.x

Papadopoulos GA, Gràcia E, Urgeles R, Sallares V, De Martini PM, Pantosti, D et al. (2014). Historical and pre-historical tsunamis in the Mediterranean and its connected seas: Geological signatures, generation mechanisms and coastal impacts. Marine Geology 354: 81–109. https://doi.org/https://doi.org/10.1016/j.margeo.2014.04.014

Power W, Clark K, King DN, Borrero J, Howarth J, Lane E et al. (2017). Tsunami runup and tide-gauge observations from the 14 November 2016 M7.8 Kaikōura earthquake, New Zealand. Pure and Applied Geophysics 174(7): 2457–2473. https://doi.org/10.1007/s00024-017-1566-2

Satake K (1994). Mechanism of the 1992 Nicaragua Tsunami Earthquake. Geophysical Research Letters 21(23): 2519–2522. https://doi.org/https://doi.org/10.1029/94GL02338

Tan O, Papadimitriou EE, Pabucçu Z, Karakostas V, Yörük A, Leptokaropoulos K (2014). A detailed analysis of microseismicity in Samos and Kusadasi (Eastern Aegean Sea) areas. Acta Geophysica 62(6): 1283–1309. https://doi.org/10.2478/s11600-013-0194-1

Tepe Ç, Sözbilir H (2017). Tectonic geomorphology of the Kemalpaşa Basin and surrounding horsts, southwestern part of the Gediz Graben, Western Anatolia. Geodinamica Acta 29(1): 70–90. https://doi.org/10.1080/09853111.2017.1317191

Thatcher W, Marshall G, Lisowski M (1997). Resolution of fault slip along the 470-km-long rupture of the great 1906 San Francisco earthquake and its implications. Journal of Geophysical Research: Solid Earth 102(B3): 5353–5367. https://doi.org/https://doi.org/10.1029/96JB03486

Ulrich T, Gabriel A-A, Ampuero, J-P, Xu W (2019a). Dynamic viability of the 2016 Mw 7.8 Kaikōura earthquake cascade on weak crustal faults. Nature Communications 10(1): 1213. https://doi.org/10.1038/s41467-019-09125-w

Ulrich T, Vater S, Madden EH, Behrens J, van Dinther Y, van Zelst I et al. (2019b). Coupled, Physics-Based Modeling Reveals Earthquake Displacements are Critical to the 2018 Palu, Sulawesi Tsunami. Pure and Applied Geophysics 176(10): 4069–4109. https://doi.org/10.1007/s00024-019-02290-5

Wu Y, Kanamori H (2005). Rapid Assessment of Damage Potential of Earthquakes in Taiwan from the Beginning of P Waves. Bulletin of the Seismological Society of America 95. https://doi.org/10.1785/0120040193.